Research Article | Vol. 28, No. 21 / 12 October 2020 / Optics Express 31043
Optics EXPRESS

Digitally tailoring arbitrary structured light of generalized ray-wave duality

ZHENSONG WAN,[1,2] ZHAOYANG WANG,[1,2] XILIN YANG,[3] YIJIE SHEN,[1,2,4,5] AND XING FU[1,2,6]

[1]*Key Laboratory of Photonic Control Technology (Tsinghua University), Ministry of Education, Beijing 100084, China*
[2]*State Key Laboratory of Precision Measurement Technology and Instruments, Department of Precision Instrument, Tsinghua University, Beijing 100084, China*
[3]*Electrical and Computer Engineering Department, University of California, Los Angeles, CA 90095, USA*
[4]*Current Address: Optoelectronics Research Centre, University of Southampton, Southampton SO17 1BJ, UK*
[5]*shenyj15@tsinghua.org.cn*
[6]*fuxing@mail.tsinghua.edu.cn*

Abstract: Structured lights, particularly those with tunable and controllable geometries, are highly topical due to a myriad of their applications from imaging to communications. Ray-wave duality (RWD) is an exotic physical effect in structured light that the behavior of light can be described by both the geometric ray-like trajectory and a coherent wave-packet, thus providing versatile degrees of freedom (DoFs) to tailor more general structures. However, the generation of RWD geometric modes requires a solid-state laser cavity with strict mechanical control to fulfill the ray oscillation condition, which limits the flexiblility of applications. Here we overcome this confinement to generate on-demand RWD geometric modes by digital holographic method in free space without a cavity. We put forward a theory of generalized ray-wave duality, describing all previous geometric modes as well as new classes of RWD geometric modes that cannot be generated from laser cavities, which are verified by our free-of-cavity creation method. Our work not only breaks the conventional cavity limit on RWD but also enriches the family of geometric modes. More importantly, it offers a new way of digitally tailoring RWD geometric modes on-demand, replacing the prior mechanical control, and opening up new possibilities for applications of ray-wave structured light.

1. Introduction

Light can be modelled as both ray and wave representations, with the ray a fundamental concept in geometric optics and used routinely in lens design, while waves apply to wave optics to describe the phenomena such as interference and diffraction. Feynman path integral theory uses the representation theory in classical optics and builds a bridge between ray and wave descriptions [1]. However in recent years, ever-increasing mesoscopic physical phenomena with exotic structured light are outdoing the scope of conventional geometric and wave optics, e.g. the wave-chaotic modes in microcavities [2,3], the dynamics of optical catastrophe [4], the structured caustics light [5,6], and ray-optical Poincaré sphere for structured Gaussian beams [7]. In order to interpret these abnormal optical modes, some new physical effects were proposed for pursuing generalized theories combining the ray-wave optics and quantum optics, such as the ray-wave duality (RWD). The effect of RWD was presented to characterize the abnormal laser mode [8–11], playing as a macroscopic manifestation of wave-particle duality in laser oscillation. The behavior of RWD geometric modes can be described on one hand by the classical ray trajectory [8], and on the other hand by a coherent wave-packet, revealing its nature parallel to the quantum coherent state where the probability wave-packet is coupled with the classical movement of the

#400587 https://doi.org/10.1364/OE.400587
Journal © 2020 Received 17 Jun 2020; revised 7 Sep 2020; accepted 20 Sep 2020; published 2 Oct 2020

Optics EXPRESS

Hamiltonian [12–15]. Recently, more and more exotic RWD geometric modes were generated based on the SU(2) coherent state [16,17], which is coupled with the classical trajectory of various linear cluster structures yielded by SU(2)-Lie algebra. For instance, the multi-path and vector geometric mode can be obtained based on the periodic oscillating ray trajectory in the laser cavity [18–20], while the emitting planar geometric mode can be transformed into structured vortex beam carrying orbital angular momentum (OAM) and coupled with the classical trajectory located on a hyperboloidal ruled surface [21,22]. By replacing the fundamental light that couples with the classical ray-orbit by the twisted light, the multi-path structured RWD geometric modes can also be generalized into multi-vortex structure [23,24]. Furthermore, RWD geometric modes with higher complexity can be realized with more controllable parameters in SU(2) coherent state, such as the 3D coherent wave-packets located on the Lissajous curve and trochoidal parametric surfaces [25–27]. These exotic RWD geometric modes largely enrich the family of structured lights with more DoFs [20]. The DoFs of RWD geometric modes include wave-packet shape, central OAM, partial OAM and coherent-state phase, and all DoFs are determined by multi-parameters of RWD geometric modes. Once multi-parameters of RWD geometric modes being freely modulated, such RWD geometric modes with salient quantum-classical coupled properties would surely broaden the related applications such as optical manipulation [28,29], quantum entanglement [30–33], particle trapping [34–36], communications [33,37], and security encryption [38,39].

Until now, unfortunately, the only way to generate geometric modes with RWD is the output from a solid-state laser cavity with a mechanical control at a frequency-degenerate state, where the ratio of transverse and longitudinal frequency spacings should be a rational number, i.e. $\Delta\omega_T/\Delta\omega_L = P/Q$ (P and Q are coprime integers). It also requires an off-axis pumping control in such a special cavity, so that the laser modes have preference to be localized on the periodic ray trajectories based on the RWD effect [12,18]. Various structured RWD geometric modes corresponding to various parameters in SU(2) coherent state were generated by precise control of cavity and pumping parameters. However, this method has inevitable obstacles: (1) the solid-state laser cavity with mechanical control devices is complicated and bulky, losing the flexibility and compactness; (2) some conditions of complex SU(2) coherent states are too strict to realize. For example, the Lissajous geometric modes need the precise control to realize a tiny difference between the cavity lengths at $x-$ and $y-$ axis direction. Therefore, it is difficult and inconvenient to generate Lissajous geometric modes. Moreover, the practical cavity length cannot be infinitely short because of crystal, thus the cases for large Q are too strict to realize; (3) it is impossible to cover all the frequency-degenerate states via cavity control, where the available values of Q are very limited. Because the actual frequency-degeneracy is controlled by cavity parameters yielded by $P/Q = (1/\pi)\cos^{-1}(1 - L/R)$, where L and R are the length and radius of curvature of the plano-concave hemispherical cavity [19], the cases for $Q \leq 2$ would result into unsteady cavities. To overcome all the drawbacks and inconveniences, it urgently calls for a free-of-cavity method of generating RWD geometric modes, breaking the bottleneck of the degenerate cavity method.

In this paper, a generalized theory of RWD geometric modes is proposed, revealing the general connection of classical trajectories and wave-packet of SU(2) coherent state, which not only covers all the geometric modes generated in a frequency degenerate cavity but also includes new classes of RWD geometric modes that cannot be produced from a cavity, e.g. the cases with Q value of 0, 1, 2 and even negative integers. On that basis, we present a method to experimentally generate the generalized RWD geometric modes by external digital holographic control, which breaks the traditional paradigm of degenerate laser cavities, and proves to be much more comprehensive, flexible, and simple. We experimentally obtained fruitful RWD geometric modes by our digital way, which allows easy access to a myriad of new modes that are either out of reach or extremely difficult to realize and control in the traditional intracavity method, thus largely enriching the family of geometric modes. More importantly, the digital on-demand RWD

Optics EXPRESS

generation scheme replacing the mechanical control opens up new possibilities for applications of ray-wave structured light in optical trapping, optical tweezers, quantum entanglement and optical communication.

2. Theory of generalized ray-wave duality

In this section, we outline the basic concepts involved in our work for a clear interpretation before introducing the theoretical model. It is known that when a laser cavity is operated in a frequency degenerate state with geometry fulfilling a ray-like periodic trajectory that oscillates back and forth as geometric optics predicts, the laser wave-packet appears to be coupled with the classical trajectory as the RWD effect [18]. Although ray-like, the laser mode can be expressed by a superposed wave-packet of various free-space Hermite–Laguerre–Gaussian (HLG) eigenmodes that demonstrated by SU(2) unitary transformation as a form of SU(2) coherent states [16,17,19,21,22]. The classical trajectories coupled with corresponding RWD wave-packet are formed by a cluster of geometric rays. Prior to this study, the actual beam shape of this superposed wave-packet is determined by adjusting the length of cavity, cavity mirror radius of curvatures, pump power and the position of the pump light, while the DoFs of the RWD effect are all confined in the cavity geometry. Here, we update the theoretical model by exploiting more quantum-classical connected properties of SU(2) coherent state and redefine the concept of RWD, so that the RWD effect is generalized beyond the limit of laser cavity.

2.1. SU(2) coherent states with quantum-classical connection

The SU(2) coherent wave-packet is the specific quantum state most closely resembling the classical state, while it is also a class of structured modes that superposed by various frequency-degenerate eigenstates. The wave packet is coupled with the classical movement yielded by the corresponding Hamiltonian. The coherent states under SU(2) symmetry group can be written as [9,16,17]:

$$|\phi\rangle = \frac{1}{2^{N/2}} \sum_{K=0}^{N} \binom{N}{K}^{1/2} \mathrm{e}^{\mathrm{i}K\phi} \, |K, N\rangle. \tag{1}$$

where N is the total bosons number, the states $|K, N\rangle$ are the states with K bosons in the first mode and $(N - K)$ bosons in the second mode [16], and ϕ is the initial phase of coherent state. The SU(2) coherent state with HLG eigenstates is given by [15,40]:

$$|\Psi^{(\alpha,\beta,\phi)}_{n_0,m_0,l_0}\rangle^{N}_{p,q} = \frac{1}{2^{N/2}} \sum_{K=0}^{N} \binom{N}{K}^{1/2} \mathrm{e}^{\mathrm{i}K\phi} |\psi^{(\alpha,\beta)}_{n_0+pK,m_0+qK,l_0-PK}\rangle. \tag{2}$$

where the HLG eigenstates $|\psi^{(\alpha,\beta)}_{n_0+pK,m_0+qK,l_0-PK}\rangle$ of separable 3D harmonic oscillator with different frequencies $\omega_x = \omega_0 - q\Delta\omega$, $\omega_y = \omega_0 + p\Delta\omega$ and ω_z along x-, y- and z- axes can be obtained, in which p and q are integers, by applying SU(2) ladder operators to Gaussian fundamental modes [15,40]:

$$|\psi^{(\alpha,\beta)}_{n,m,l}\rangle = \frac{(b_x^{\dagger})^n}{\sqrt{n!}} \frac{(b_y^{\dagger})^m}{\sqrt{m!}} \frac{(b_z^{\dagger})^l}{\sqrt{l!}} |0, 0, 0\rangle, \tag{3}$$

$$\begin{bmatrix} b_x^{\dagger} \\ b_y^{\dagger} \\ b_z^{\dagger} \end{bmatrix} = \begin{bmatrix} \mathrm{e}^{-\mathrm{i}\alpha/2}\cos(\beta/2) & \mathrm{e}^{\mathrm{i}\alpha/2}\sin(\beta/2) & 0 \\ -\mathrm{e}^{-\mathrm{i}\alpha/2}\sin(\beta/2) & \mathrm{e}^{\mathrm{i}\alpha/2}\cos(\beta/2) & 0 \\ 0 & 0 & 1 \end{bmatrix} \begin{bmatrix} a_x^{\dagger} \\ a_y^{\dagger} \\ a_z^{\dagger} \end{bmatrix}, \tag{4}$$

where $a_i^{\dagger}$ $(i = x, y, z)$ are the creation operators for generating high order transverse and longitudinal mode, (α, β) are the two parametric rotation angles in SU(2) symmetry along z-axis, (n, m) and l

Optics EXPRESS

are transverse and longitudinal mode indices, respectively. Of particular note, when $\alpha(\beta) = 0$ or π, $|\psi^{(\alpha,\beta)}_{n,m,l}\rangle$ is reduced into HG modes; when $\alpha = \beta = \pm\pi/2$, $|\psi^{(\alpha,\beta)}_{n,m,l}\rangle$ is reduced into LG modes. The eigenstates with SU(2) transformation can well represent various HLG eigenmodes. The theoretical SU(2) coherent states with different rotation angles (α, β) and initial phase ϕ are shown in Fig. 1(a) and (b), respectively.

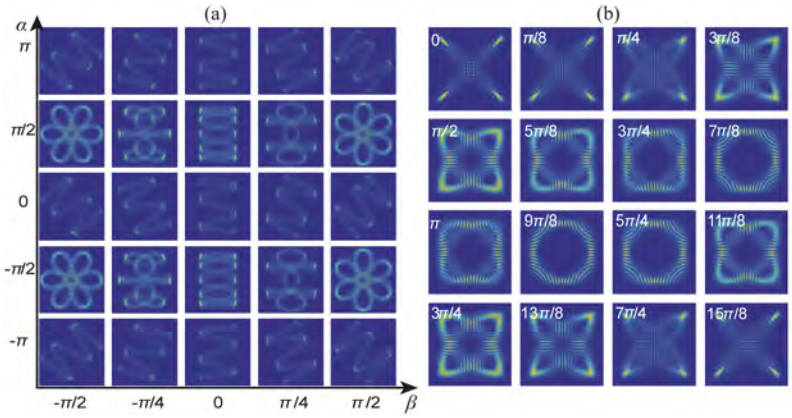

Fig. 1. Intensity pattern of SU(2) coherent states. (a) $|\Psi^{(\alpha,\beta,0)}_{20,20,l}\rangle^{5}_{-1,5}$. (b) $|\Psi^{(0,0,\phi)}_{20,20,l}\rangle^{10}_{2,2}$.

As a salient property of SU(2) coherent state, the probability wave-packet is coupled with the classical movement [14,15]. The wave-packet of the SU(2) coherent state is always located on the corresponding trajectory [8]. The trajectory of classical movement of the separable 3D transversely symmetric harmonic oscillator $(x^{\pm}_{a,k}, y^{\pm}_{a,k}, z^{\pm}_{a,k})$ yields [41]:

$$\begin{cases} x^{\pm}_{a,k} = \sqrt{N_x} w(z) \cos\left[2\pi k \dfrac{\omega_x}{\omega_z} + \phi_x \pm \vartheta(z)\right] \\ y^{\pm}_{a,k} = \sqrt{N_y} w(z) \cos\left[2\pi k \dfrac{\omega_y}{\omega_z} + \phi_y \pm \vartheta(z)\right] \\ z^{\pm}_{a,k} = z \end{cases} \tag{5}$$

where the integer $k = 0, 1, 2, \ldots$ is the running index for the caustics cluster of rays, (N_x, N_y) and (ϕ_x, ϕ_y) are the intensities and initial phases of oscillator components at x- and y-axis respectively, $w(z) = w_0\sqrt{1 + (z/z_R)}$ is Gaussian beam waist parameter, and $\vartheta(z) = \tan^{-1}(z/z_R)$ is Gouy phase where z_R is the Rayleigh range. N_x and N_y are positively correlated with n_0 and m_0, and $\phi_x - \phi_y = \phi$. The symbol + and − respresent the forward and backward rays, respectively. Hereinafter, we omit the notation symbol ± of the classical trajectories.

The SU(2) transformation of the trajectory $(x_{a,k}, y_{a,k}, z_{a,k})$ is coupled with that of operator transformation of Eq. (4), and the SU(2) coherent states wave-packet would be located along the SU(2) classical trajectory of $(x_{b,k}, y_{b,k}, z_{b,k})$ [14,15], demonstrating quantum-classical connection [13]. Utilizing SU(2) transformation, the expression of (x_b, y_b, z_b) can be expressed as:

$$\begin{bmatrix} x_b \\ y_b \\ z_b \end{bmatrix} = \begin{bmatrix} e^{-i\alpha/2}\cos(\beta/2) & e^{i\alpha/2}\sin(\beta/2) & 0 \\ -e^{-i\alpha/2}\sin(\beta/2) & e^{i\alpha/2}\cos(\beta/2) & 0 \\ 0 & 0 & 1 \end{bmatrix} \begin{bmatrix} x_a \\ y_a \\ z_a \end{bmatrix}, \tag{6}$$

The classical trajectory (x_b, y_b, z_b) with different values of (α, β) corresponds to the SU(2) coherent state wave-packet with HLG eigenstates of Eq. (2).

Optics EXPRESS

In short, the eigenstates of 3D separable harmonic oscillators are HG modes in the Cartesian coordinate system, and the corresponding classical motion trajectory is the Lissajous curve, while the coherent state wave-packet with HG eigenstates is coupled with the classical trajectory. The general HLG eigenstate between HG and LG eigenstate can be obtained by applying SU(2) unitary transformation on ladder operators, and the coherent state with HLG eigenstates can be called as SU(2) coherent state. Meanwhile, the family of the classical trajectory with continuous-transformation orbits between Lissajous and trochoidal curves can be obtained by applying SU(2) transformation on the Lissajous curve [41]. Hereto, the SU(2) coherent states with classical quantum coupling have been clarified.

2.2. Generalized ray-wave duality

Based on the SU(2) coherent states of Eq. (2) with the coupled SU(2) classical trajectory given by Eq. (5), we can propose our new definition of RWD. When the ratio of ω_x/ω_z or ω_y/ω_z is an irrational number, the trajectories of $(x_{b,k}, y_{b,k}, z_{b,k})$ would not be overlapped to each other and can constitute a continuous spatial surface with the running of k to infinity [12], thus no RWD effect in this case. Whereas if the ratios of ω_x/ω_z and ω_y/ω_z are rational numbers, the trajectory of $(x_{b,k}, y_{b,k}, z_{b,k})$ just represents a ray cluster with a limited number of rays because the trajectory would coincide with itself having k running for certain period, with the examples of classical trajectory shown in Fig. 2, and the spatial wave-packet of corresponding SU(2) coherent state is localized on this trajectory, which embodies the quantum-classical connection and namely the RWD effect. In general, the RWD effect reveals the coupled effect of light ray trajectory and wave-packet, the definition and working principle of which is independent of laser cavity. Meanwhile, SU(2) coherent states are a rich class of RWD geometric modes.

Hereinafter we derive some special sets of the RWD geometric modes:

1. ***Lissajous-to-trochoidal parametric surface mode*** **:** For the special case of $\omega_0/\omega_z = P/Q$ and $\Delta\omega/\omega_0 = M_1/M_2$ where (P, Q) and (M_1, M_2) are two pairs of coprime integers, it can be derived that $\omega_x/\omega_z = P/Q(1 - qM_1/M_2)$ and $\omega_y/\omega_z = P/Q(1 + pM_1/M_2)$ are two rational numbers, and the classical trajectory as described by Eq. (5) is reduced into a caustics cluster with limited rays. As shown in the first row of Fig. 2, the SU(2) classical trajectory $(x_{b,k}, y_{b,k}, z_{b,k})$ $(k = 0, 1, 2, \ldots, |QM_2| - 1)$ with different values of (α, β) represents respectively a caustics cluster including $|QM_2|$ rays uniformly distributed on a Lissajous parametric surface $(\alpha = \beta = 0)$ [25], trochoid parametric surface $(\alpha = \beta = \pi/2)$ [26] and the topological SU(2) surface interposed between Lissajous and trochoidal parametric surfaces (the case shown with $\alpha = \pi/2, \beta = \pi/4$). The general expressions of the illustrated three scenarios of classical trajectory are given in the first row as well. Moreover, at a certain transverse plane, the transverse pattern illustrates multiple dots uniformly distributed on a certain Lissajous and trochoid curve. The corresponding SU(2) coherent states (as shown in the fourth row of Fig. 2) as denoted by Eq. (2) harnesses the wave-packet located on the 3D Lissajous-to-trochoidal parametric surface, and the wave-packet cross section located on the corresponding contour curve of the Lissajous-to-trochoidal parametric surface [40]. Especially, the wave-packet of Lissajous parametric surface modes with different ϕ have different shape, as shown in Fig. 1(a). Meanwhile, the wave-packet of trochoidal parametric surface modes with different ϕ are rotating with each other. The total OAM of Lissajous and trochoidal parametric surface mode are 0 and $|n_0 + pN - m_0 - qN|$, respectively.

2. ***Multi-axis Hermite–Laguerre–Gaussian mode*****:** For a special case of $p = Q$, $q = 0$, and $s = -P$, the SU(2) classical trajectory is no longer along a Lissajous-trochoidal curve but reduced to compose multiple linear oscillation orbits in a certain transverse plane. The SU(2) classical trajectory has the axes located on a main uniparted hyperboloid ruled surface [23], composing a SU(2) symmetric structure, as shown in the second row of Fig. 2. The corresponding SU(2) coherent states wave-packet (as shown in the fifth row of Fig. 2) harnesses multi-axis HLG mode, where the multiple sub-HLG modes propagating along the $|Q|$ axes are uniformly distributed

Optics EXPRESS

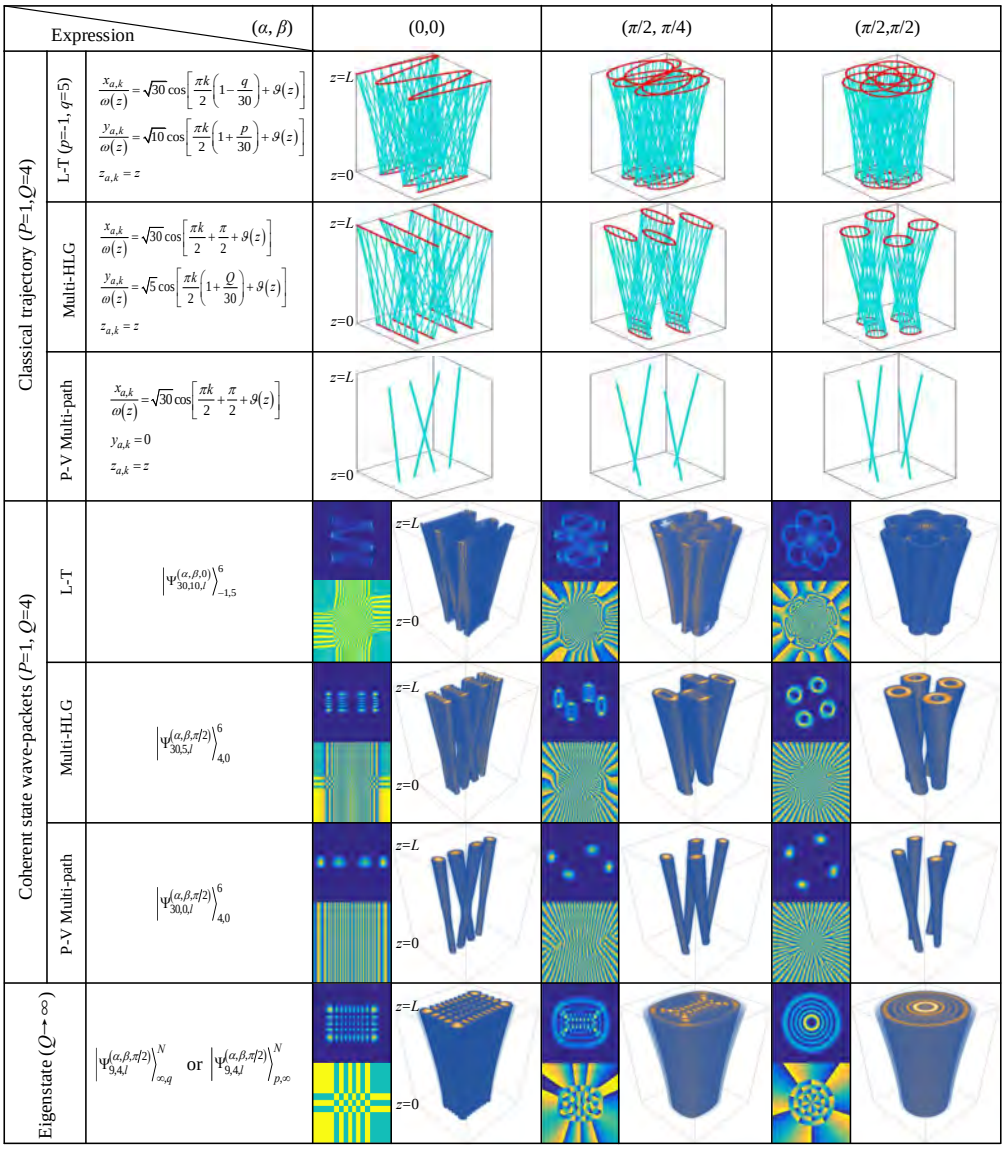

Fig. 2. The evolution of theoretical wave-packets and classical trajectories of RWD geometric modes from $z = 0$ to $z = L$), where $L = z_R \tan[\pi P/(p + q)]$ (z_R is the Rayleigh range of eigenstate). Classical trajectories ($(x_{b,k}, y_{b,k}, z_{b,k})$) can be derived by plugging corresponding ($(x_{a,k}, y_{a,k}, z_{a,k})$) and (α, β) into the Eq. (6). The general Lissajous-to-trochoidal (L-T) parametric surface mode degenerates to multi-axis HLG mode with the parameters (p,q,n_0,m_0), then to planar-to-vortex (P-V) multi-path geometric mode, even to eigenstate ($Q \to \infty$) respectively. The 2D wave patterns and phase distributions presented here are corresponding to transverse modes in $z = 0$ plane. (Colormap: darkness to brightness means 0 to 1 a.u. for intensity, and $-\pi$ to π for phase.)

coherent states wave-packet (as shown in the fifth row of Fig. 2) harnesses multi-axis HLG mode, where the multiple sub-HLG modes propagating along the $|Q|$ axes are uniformly distributed on the main uniparted hyperboloid ruled surface. Specially, the topological charge of a sub-LG

Optics EXPRESS

on the main uniparted hyperboloid ruled surface. Specially, the topological charge of a sub-LG mode vortex is equal to m_0 in the multi-axis LG mode ($\alpha = \beta = \pi/2$), the center topological charge of the main vortex is equal to n_0, and that for the partial phase singularities is $|QN|$ that lie at the midpoint of the line between the two adjacent rays. The total OAM of multi-axis HG and LG modes are 0 and $|n_0 + QN - m_0|$, respectively.

3. *Planar–to-vortex multi–path geometric mode*: For a more special instance of $N_y = m_0 = q = M_1 = 0$, $p = Q$, the corresponding SU(2) trajectory is shown in the third row of Fig. 2, which is actually the $|Q|$ rays uniformly distributed on a uniparted hyperboloid ruled surface [19]. Meanwhile, the corresponding SU(2) coherent states wave-packet (as shown in the sixth row of Fig. 2) can be obtained by replacing the sub-HLG beams in the multi-axis HLG modes by fundamental Gaussian beams. For a vortex multi-path geometric mode ($\alpha = \beta = \pi/2$), the topological charge of the center vortex and the partial phase singularities is same with multi-axis LG mode. The total OAM of planar and vortex multi-path geometric modes are 0 and $|n_0 + QN|$, respectively.

4. *From ray-wave duality to eigenstate*: For an even further special case when $|Q| \to \infty$, the ratio of ω_0/ω_z is approaching an irrational number [12]. There would be infinite rays in the SU(2) classical trajectory of Eq. (5) covering the whole internal region of a hyperbola, and the corresponding SU(2) coherent states is reduced into an eigenstate HG mode. After the SU(2) transformation, the rays in the SU(2) classical trajectory $(x_{b,k}, y_{b,k}, z_{b,k})$ would cover the whole surface of an uniparted hyperboloid, and the corresponding SU(2) coherent states is reduced into an eigenstate HLG or LG vortex mode ($\alpha = \beta = \pm\pi/2$). This process subtly reveals the nature of photons traveling along straight lines in arbitrary formation of various basic vortex modes in free-space.

Hereto, we have introduced four types of SU(2) coherent state with different (p, q), (n_0, m_0) and N. All the Lissajous-to-trochoidal parametric surface modes, multi-axis Hermite-Laguerre-Gaussian modes, planar-to-vortex multi-path geometric modes, and eigenstate modes can be described by the generalized RWD theorem presented here. We have made further discussion on the classical trajectory and the corresponding wave-packets for all above modes. In nature, the SU(2) coherent states degenerates from Lissajous and trochoidal parametric surfaces mode state into an eigenstate as the frequency-degenerate condition degrades (see Supplementary materials).

2.3. Breaking the limitation of frequency-degenerate cavity

We have established a generalized RWD theorem including many special characteristic RWD geometric modes families that the spatial wave-packet of the structured beam is always coupled with a cluster of rays. Here, we show that the generalized RWD geometric modes include the new modes that cannot be generated by prior method. Conventionally, the realization of RWD geometric modes must require a laser cavity with precise control. A certain frequency-degenerate state is a necessity obtained by precisely adjusting the cavity length L and radius of curvature R of concave mirror in the equivalent confocal cavity, thus the mode-spacing ratio is related to the cavity parameters by [19]:

$$\frac{\omega_0}{\omega_z} = \frac{P}{Q} = \frac{1}{\pi}\cos^{-1}\sqrt{1 - \frac{L}{R}}. \tag{7}$$

In this condition, multi-path geometric mode can be generated by adjusting the cavity and pumping parameters to meet the periodic oscillation ray paths as shown in Fig. 3(a). However, according to the stability requirement, the available range of L/R is limited as $0<1 - L/R<1$, thus the ratio of P/Q is severely limited as $0<P/Q<1/2$. In another word, it is impossible to generate from cavity the RWD geometric modes with the ratio of P/Q beyond the range of $(0, 1/2)$, including several special and interesting conditions such as $P/Q = 1/2$, $P/Q = 1/1$, and even Q value of zero or negative integers. Furthermore, in order to generate Lissajous-to-trochoidal parametric surface modes in experiment, the previous method calls for demanding precise control

Optics EXPRESS

to introduce astigmatism at two orthogonal directions. One can imagine that it is also impossible to simultaneously control the cavity length both at x- and y-directions to fulfill all the values of p and q, because very limited difference of cavity length can be realized in the experiment, i.e. it should be $\Delta L_x \ll L$ and $\Delta L_y \ll L$. Moreover, it suffers from the requirement that the frequency-degenerate condition should always be met in the meantime of precise adjustment of cavity. In addition, as far as we know, RWD geometric modes based on non-HG eigenstates have not been obtained directly from the cavity, which depends on the astigmatic mode converter outside the cavity.

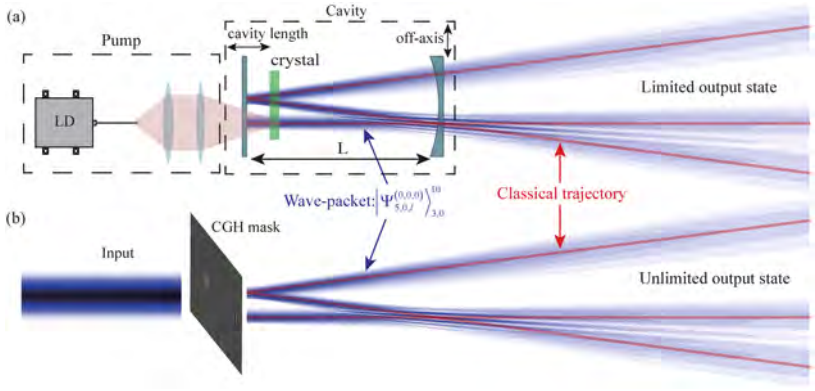

Fig. 3. Schematic diagram of our digital modulation method for generating RWD geometric modes, compared with that of cavity method.

In order to break the limit exerted by the stability criterion of frequency-degenerate cavity, we put forward a free-of-cavity method to produce and tailor RWD geometric modes, which enjoys much more degrees of freedom as well as dramatically enhanced flexibility, simplicity and integrity. Furthermore, those exotic RWD geometric modes with extreme parameters such as $P/Q = 1/2$, $P/Q = 1/1$, and even Q value of zero or negative integers are included in our new theoretical model.

3. Realization of generalized ray-wave duality modes on demand

In this section, we demonstrate the realization of generalized RWD geometric modes experimentally, free of limits exerted by the cavity. The SU(2) coherent states as described by Eq. (2) are superposed by various frequency-degenerate eigenstates, and the shape of wave-packets depends on the superposed transverse modes components. The idea of our method is to do complex amplitude modulation to tailor superposed targeted transverse pattern, and the wave packet formed during the propagation can be coupled with the corresponding classical trajectory, as shown in Fig. 3(b). This mimics the mechanism of laser cavity: creating patterns and different angle of propagation from the output coupler. The phase mask of arbitrary RWD geometric can generated by the phase-only computer generated hologram (CGH) method [42,43], which break the cavity limit. Specifically, in our method, as Fig. 3(b) shows, arbitrary RWD geometric modes can be easily generated by modulating a fundamental Gaussian beam with a spatial light modulator (SLM) that is loaded with the phase mask of required RWD geometric modes. Then the target SU(2) coherent state beam can be obtained by separating it from the modulated Gaussian beam.

3.1. Experimental setup

In our experimental setup as shown in Fig. 4, a near-HG_{00} mode produced by the 1064-nm laser source (2W) was adjusted to be s-polarized by passing through a linear polarizer and a half-wave

Optics EXPRESS

plate in succession. Then the beam was expanded by a telescope (L1, focal length of 20 mm; L2, focal length of 120 mm) with the magnification of 1:6 to become a near-plane wave. After passing through a beam splitter (BS), the near-plane wave illuminated a reflective phase-only SLM (Meadowlark Optics, 1920×1152 pixels, liquid crystal on silicon), which is loaded with the hologram phase mask generated by CGH method. Finally, the light field modulated by SLM was focused by a lens (L3) with the focal length of 120 mm and an aperture placed at the Fourier plane, to extract the first-order spatial frequency as the target RWD beams. A charge-coupled device (CCD) camera (Spiricon, M2-200s) was used to record the pattern of RWD geometric modes in different axial position, with a lens (L4, focal length of 60 mm) to adjust the waist size and position in z-axis. Limited by the modulation efficiency of CGH method, the power of RWD geometric modes obtained is tens of milliwatts. Specifically, arbitrary RWD geometric beams can be obtained by changing hologram phase mask in SLM in a digital way, which makes our approach extremely flexible and stable. Figure 4 depicts an RWD beam ($|\Psi^{(0,0,\pi/2)}_{20,10,l}\rangle^{5}_{-3,4}$) that cannot be generated by the cavity method.

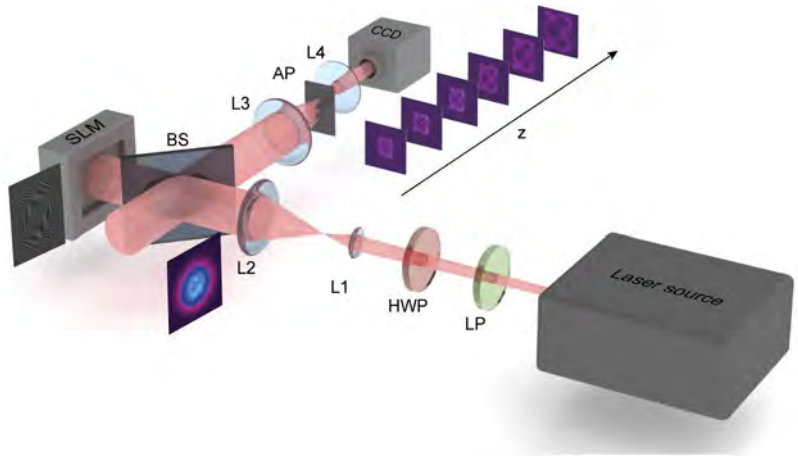

Fig. 4. Experimental setup. HWP, half-wave plate; LP, linear polarizer; L1-L4, lens; BS, beam splitter; SLM, spatial light modulator; AP: Aperture; CCD, charge coupled device.

3.2. Results and discussions

Hereinafter, we demonstrate the experimental result of generalized RWD geometric modes, including Lissajous and trochoidal parametric-surface modes, multi-axis HLG, planar-to-vortex multi-path geometric modes and RWD geometric modes that break the bottleneck of cavity. Beside, all set of parameters of the generalized RWD geometric modes described in Eq. (2) can be controlled at will. The control of rotation parameters of SU(2) rotation angles α and β, the initial transverse mode order n_0, m_0 and initial phase ϕ, transversely coupled parameters p and q, and the total bosons number N are also demonstrated. In this manner, different RWD geometric modes can be rapidly and successively generated at ease, simply by switching the SLM masks.

1. ***Realization of RWD geometric modes*****:** Lissajous and trochoidal parametric-surface modes, as the most general modes represented by SU(2) coherent states in Eq. (2), are obtained in the experiment, as shown in Fig. 5(a, d). The left, middle and right rows of each sub-figure display the classical trajectories, experimental and theoretical patterns respectively. The experimental results of mode intensity distribution are obtained at every transverse plane, demonstrating the mode pattern evolution along the propagation from $z = 0$ to $z = L$. These results all agree well with the theoretical wave-packets and classical trajectories, verifying the validity and stability of our method of realizing the quantum-classical connection without cavity.

Optics EXPRESS

Figures 5(b, e) and (c, f) demonstrate the experiment results of multi-axis HLG mode and planar-to-vortex multi-path geometric mode, respectively. There are Q sub-HLG and Q sub-path Gaussian beams along the Q axes uniformly distributed on the cross section. It should be noted that the multiple-axis HLG beams are coherently composed by multiple sub-HLG beams, while the multi-path geometric beams are coherently composed by multiple sub-fundamental beams. When the sub-HLG beams are replaced by sub-fundamental beams, the multi-axis HLG beams are reduced into multi-path geometric beams. Specifically, multi-axis HLG and multi-path geometric beams would rotate around the center axis when $\alpha \neq \pi/2$ and $\beta \neq \pi/2$, indicating the existence of OAM in the beam center.

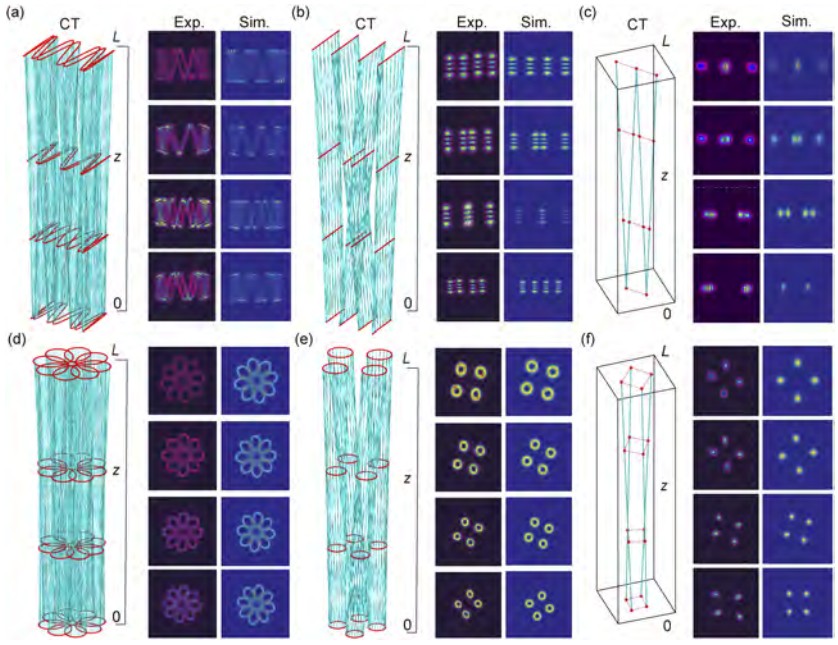

Fig. 5. Propagation evolution of classical trajectory, experimental and theoretical wavepackets of Lissajous (a) and trochoidal (d) parametric-surface modes, multi-axis HLG modes (b,e) and planar-to-vortex multi-path geometric modes(c,f) with different parameters. (a) $|\Psi^{(0,0,\pi/4)}_{15,20,l}\rangle^{10}_{-1,7}$. (b) $|\Psi^{(0,0,\pi/2)}_{10,3,l}\rangle^{5}_{4,0}$. (c) $|\Psi^{(0,0.\pi)}_{10,0,l}\rangle^{5}_{4,0}$. (d) $|\Psi^{(\pi/2,\pi/2,\pi/4)}_{15,20,l}\rangle^{10}_{1,5}$. (e) $|\Psi^{(\pi/2,\pi/2,\pi/2)}_{15,3,l}\rangle^{5}_{4,0}$. (f) $|\Psi^{(\pi/2,\pi/2,\pi)}_{10,0,l}\rangle^{5}_{4,0}$.

The RWD geometric mode generator and mode switch undoubtedly provides a powerful tool for applications such as optical tweezers and macromolecule assembly, taking advantage of the unique phase and intensity distribution of a variety of three-dimensional SU(2) coherent states. The generalized RWD geometric modes naturally has multiple DoFs, which is extremely advantageous for potential applications such as communications.

2. ***Realization of RWD geometric modes that break the bottleneck of cavity*****:** The experimental realization of the modes that are unprocurable from cavity method are demonstrated in Fig. 6 for the cases of $Q = 2$, $Q = 1$ and $Q = 0$, along with the theoretical patterns. The experimental results of mode evolution along the propagation from $z = 0$ to $z = z_R$ are obtained because there is no corresponding length in a real cavity for $Q \leqslant 2$. It can be seen that the cone-like propagation trail, fidget-spinner-like beams, and square-shaped beams can be obtained for the cases of $Q = 2$, 1 and 0, respectively. The results also show that OAM exists in several modes, as revealed by the pattern rotation along the beam propagation. Especially, there are no

Optics EXPRESS

classical trajectory for $Q = 0$, and SU(2) coherent state shows the characteristic of the propagation in-variance. Moreover, there are still numerous peculiar beams as generalized RWD geometric modes yet to be explored and unraveled, potentially opening broader space for the applications of structured lights in the future. The most significant advantage of producing RWD geometric modes without cavity is the flexibility and convenience. Experimental results of dynamically

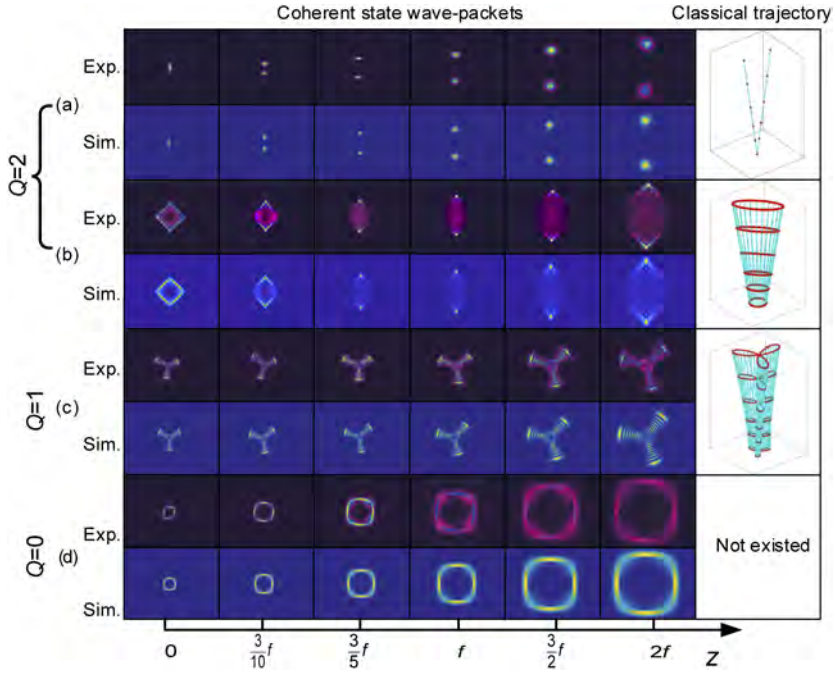

Fig. 6. Experimental and theoretical results of the propagation evolution of transverse patterns for $Q = 2$, $Q = 1$ and $Q = 0$ with different parameters. (a) $|\Psi^{(0,0,\pi)}_{10,0,l}\rangle^{5}_{2,0}$. (b) $|\Psi^{(0,0,\pi)}_{10,10,l}\rangle^{5}_{1,1}$. (c) $|\Psi^{(\pi/2,\pi/2,\pi/2)}_{10,10,l}\rangle^{5}_{-1,2}$. (d) $|\Psi^{(0,0,3\pi/2)}_{20,10,l}\rangle^{5}_{-1,1}$.

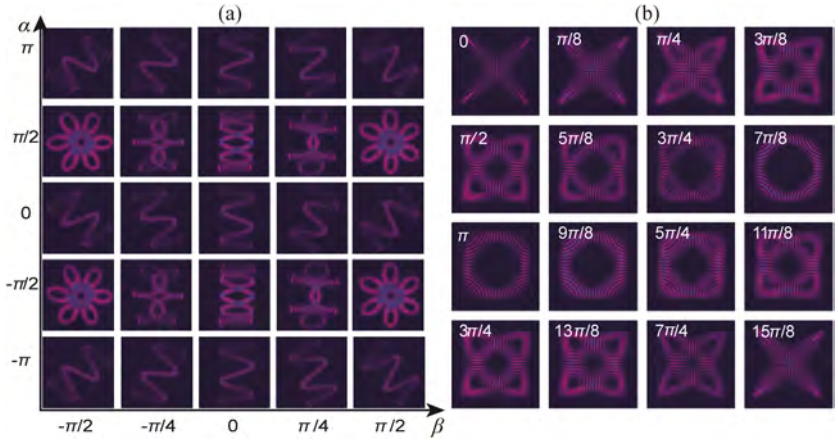

Fig. 7. Experimental results as examples of digital parameter control on RWD geometric modes. (a) $|\Psi^{(\alpha,\beta,0)}_{20,20,l}\rangle^{5}_{-1,5}$. (b) $|\Psi^{(0,0,\phi)}_{20,20,l}\rangle^{10}_{2,2}$.

Optics EXPRESS

controlling more parameters(α, β, ϕ) are provided in Fig. 7, as examples of our method of generating and controlling RWD geometric modes on-demand.

4. Conclusion

In summary, the generalized RWD geometric modes are presented in theory and realized in experiment, which cover not only the previous reported geometric modes such as Lissajous to trochodial parametric, multi-axis HLG and multi-path geometric modes, but also new classes of RWD geometric modes that cannot be generated from the cavity, e.g. modes with Q value of 0, 1, 2 and even negative integers, breaking the cavity limit on RWD geometric modes and enriching the family of geometric mode. In addition, the peculiarity of trajectories and wave-packet of SU(2) structured light are demonstrated. Moreover, our way of producing generalized RWD geometric modes is surprisingly simple, employing the CGH method and a compact setup with SLM. We also note that the holography generation scheme has large scalability, which are also available to be realized by other hologram devices besides SLM such as the digital micromirror devices [44,45]. The free-of-cavity method demonstrates a fundamental shift in paradigm of obtaining and manipulating RWD geometric modes, and offers a way of tailoring, dynamically and flexibly controlling the RWD geometric modes on-demand, which paves the route to extend quantum coherence state modes as a powerful and customized toolbox into applications such as quantum entanglement, optical tweezers, and optical communication.

Funding

National Key Research and Development Program of China (2017YFB1104500); National Natural Science Foundation of China (61975087); Beijing Young Talents Support Project (2017000020124G044); Marie S.-Curie MULTIPLY Fellowship (GA713694).

Disclosures

The authors declare no conflicts of interest.

See Supplement 1 for additional details of eigenstates of harmonic oscillator in quantum optics, the classical trajectory and wave-packet of RWD geometric modes as well as the method of simulation. The phase mask design of generalized RWD geometric modes is also described in detail in Supplementary materials.

References

1. J. Babington, "Ray-wave duality in classical optics: crossing the feynman bridge," Opt. Lett. **43**(22), 5591–5594 (2018).
2. S. Bittner, S. Guazzotti, Y. Zeng, X. Hu, H. Yılmaz, K. Kim, S. S. Oh, Q. J. Wang, O. Hess, and H. Cao, "Suppressing spatiotemporal lasing instabilities with wave-chaotic microcavities," Science **361**(6408), 1225–1231 (2018).
3. H. Cao, R. Chriki, S. Bittner, A. A. Friesem, and N. Davidson, "Complex lasers with controllable coherence," Nat. Rev. Phys. **1**(2), 156–168 (2019).
4. A. Zannotti, F. Diebel, and C. Denz, "Dynamics of the optical swallowtail catastrophe," Optica **4**(10), 1157–1162 (2017).
5. H. Peng and H. Chen, "Caustics from optical conformal mappings," Phys. Rev. Appl. **12**(6), 064030 (2019).
6. A. Zannotti, C. Denz, M. A. Alonso, and M. R. Dennis, "Shaping caustics into propagation-invariant light," Nat. Communications **11**, 3597 (2020).
7. M. A. Alonso and M. R. Dennis, "Ray-optical poincaré sphere for structured gaussian beams," Optica **4**(4), 476–486 (2017).
8. N. Barré, M. Romanelli, M. Lebental, and M. Brunel, "Waves and rays in plano-concave laser cavities: I. geometric modes in the paraxial approximation," Eur. J. Phys. **38**(3), 034010 (2017).

Optics EXPRESS

9. Y. F. Chen, C. H. Jiang, Y. P. Lan, and K. F. Huang, "Wave representation of geometrical laser beam trajectories in a hemiconfocal cavity," Phys. Rev. A **69**(5), 053807 (2004).
10. D. R. Herriott and H. J. Schulte, "Folded optical delay lines," Appl. Opt. **4**(8), 883 (1965).
11. I. A. Ramsay and J. J. Degnan, "A ray analysis of optical resonators formed by two spherical mirrors," Appl. Opt. **9**(2), 385–398 (1970).
12. Y. Chen, S. Li, Y. Hsieh, J. Tung, H. Liang, and K. Huang, "Laser wave-packet representation to unify eigenmodes and geometric modes in spherical cavities," Opt. Lett. **44**(11), 2649–2652 (2019).
13. R. Blumel, *Advanced quantum mechanics: the classical-quantum connection* (Jones &Bartlett Publishers, 2011).
14. S. Roy and V. Singh, "Generalized coherent states and the uncertainty principle," Phys. Rev. D **25**(12), 3413–3416 (1982).
15. J. G. Hartley and J. R. Ray, "Coherent states for the time-dependent harmonic oscillator," Phys. Rev. D **25**(2), 382–386 (1982).
16. V. Bužek and T. Quang, "Generalized coherent state for bosonic realization of su (2) lie algebra," J. Opt. Soc. Am. B **6**(12), 2447–2449 (1989).
17. K. Wodkiewicz and J. Eberly, "Coherent states, squeezed fluctuations, and the su (2) am su (1, 1) groups in quantum-optics applications," J. Opt. Soc. Am. B **2**(3), 458–466 (1985).
18. Y. Chen, J. Tung, P. Chiang, H. Liang, and K. Huang, "Exploring the effect of fractional degeneracy and the emergence of ray-wave duality in solid-state lasers with off-axis pumping," Phys. Rev. A **88**(1), 013827 (2013).
19. Y. Shen, X. Yang, X. Fu, and M. Gong, "Periodic-trajectory-controlled, coherent-state-phase-switched, and wavelength-tunable su (2) geometric modes in a frequency-degenerate resonator," Appl. Opt. **57**(32), 9543–9549 (2018).
20. Y. Shen, X. Yang, D. Naidoo, X. Fu, and A. Forbes, "Structured ray-wave vector vortex beams in multiple degrees of freedom from a laser," Optica **7**(7), 820–831 (2020).
21. Y. Shen, Z. Wan, Y. Meng, X. Fu, and M. Gong, "Polygonal vortex beams," IEEE Photonics J. **10**(4), 1–16 (2018).
22. Y. Shen, X. Fu, and M. Gong, "Truncated triangular diffraction lattices and orbital-angular-momentum detection of vortex su (2) geometric modes," Opt. Express **26**(20), 25545–25557 (2018).
23. T.-H. Lu, Y. Lin, Y. Chen, and K. Huang, "Generation of multi-axis laguerre–gaussian beams from geometric modes of a hemiconfocal cavity," Appl. Phys. B **103**(4), 991–999 (2011).
24. P. Tuan, Y. Hsieh, Y. Lai, K. Huang, and Y. Chen, "Characterization and generation of high-power multi-axis vortex beams by using off-axis pumped degenerate cavities with external astigmatic mode converter," Opt. Express **26**(16), 20481–20491 (2018).
25. Y. Chen, T.-H. Lu, K. Su, and K. Huang, "Devi's staircase in three-dimensional coherent waves localized on lissajous parametric surfaces," Phys. Rev. Lett. **96**(21), 213902 (2006).
26. T.-H. Lu, Y. Lin, Y. Chen, and K. Huang, "Three-dimensional coherent optical waves localized on trochoidal parametric surfaces," Phys. Rev. Lett. **101**(23), 233901 (2008).
27. Y. Chen, Y. Lin, K. Huang, and T.-H. Lu, "Spatial transformation of coherent optical waves with orbital morphologies," Phys. Rev. A **82**(4), 043801 (2010).
28. Y. Shen, X. Wang, Z. Xie, C. Min, X. Fu, Q. Liu, M. Gong, and X. Yuan, "Optical vortices 30 years on: Oam manipulation from topological charge to multiple singularities," Light: Sci. Appl. **8**(1), 90 (2019).
29. S. Wei, G. Si, M. Malek, S. K. Earl, L. Du, S. S. Kou, X. Yuan, and J. Lin, "Toward broadband, dynamic structuring of a complex plasmonic field," Sci. Adv. **4**(6), eaao0533 (2018).
30. M. Kim, W. Son, V. Bužek, and P. Knight, "Entanglement by a beam splitter: Nonclassicality as a prerequisite for entanglement," Phys. Rev. A **65**(3), 032323 (2002).
31. G. S. Agarwal and J. Banerji, "Entanglement by linear su (2) transformations: generation and evolution of quantum vortex states," J. Phys. A: Math. Gen. **39**(37), 11503–11519 (2006).
32. Y. Li and C. Wu, "High-dimensional topological insulators with quaternionic analytic landau levels," Phys. Rev. Lett. **110**(21), 216802 (2013).
33. J. Wang, "Advances in communications using optical vortices," Photonics Res. **4**(5), B14–B28 (2016).
34. H. He, M. Friese, N. Heckenberg, and H. Rubinsztein-Dunlop, "Direct observation of transfer of angular momentum to absorptive particles from a laser beam with a phase singularity," Phys. Rev. Lett. **75**(5), 826–829 (1995).
35. D. G. Grier, "A revolution in optical manipulation," Nature **424**(6950), 810–816 (2003).
36. D. Akamatsu and M. Kozuma, "Coherent transfer of orbital angular momentum from an atomic system to a light field," Phys. Rev. A **67**(2), 023803 (2003).
37. B. Stoklasa, L. Motka, J. Rehacek, Z. Hradil, L. L. Sánchez-Soto, and G. Agarwal, "Experimental violation of a bell-like inequality with optical vortex beams," New J. Phys. **17**(11), 113046 (2015).
38. H. Ren, G. Briere, X. Fang, P. Ni, R. Sawant, S. Héron, S. Chenot, S. Vézian, B. Damilano, and V. Brändli, "Metasurface orbital angular momentum holography," Nat. Commun. **10**(1), 2986 (2019).
39. X. Fang, H. Ren, and M. Gu, "Orbital angular momentum holography for high-security encryption," Nat. Photonics **14**(2), 102–108 (2020).
40. Y. F. Chen, J. Tung, P. Tuan, and K. F. Huang, "Symmetry breaking induced geometric surfaces with topological curves in quantum and classical dynamics of the su (2) coupled oscillators," Ann. Phys. **529**(10), 1600253 (2017).
41. Y. F. Chen, "Geometry of classical periodic orbits and quantum coherent states in coupled oscillators with su (2) transformations," Phys. Rev. A **83**(3), 032124 (2011).

Optics EXPRESS

42. V. Arrizón, U. Ruiz, R. Carrada, and L. A. González, "Pixelated phase computer holograms for the accurate encoding of scalar complex fields," J. Opt. Soc. Am. A **24**(11), 3500–3507 (2007).
43. C. Rosales-Guzmán and A. Forbes, *How to shape light with spatial light modulators* (SPIE, 2017).
44. Y.-X. Ren, R.-D. Lu, and L. Gong, "Tailoring light with a digital micromirror device," Ann. Phys. **527**(7-8), 447–470 (2015).
45. S. Scholes, R. Kara, J. Pinnell, V. Rodríguez-Fajardo, and A. Forbes, "Structured light with digital micromirror devices: a guide to best practice," Opt. Eng. **59**(4), 041202 (2019).